

Supplementary Information

Liquid crystal hydroglass formed via phase separation of nanocellulose colloidal rods

Yuan Xu, Aleks Atrens, Jason R Stokes*

This file includes:

Method

Supplementary Text

Supplementary Fig. S1-S6

Method

The nanocrystalline cellulose (NCC) used was sourced from Maine University Process Development Centre (Orono, ME) as 11.9 wt% NCC aqueous suspension with 0.9 wt% sulfur on dry NCC sodium form which is equivalent to 4.62 SO_3^- per 100 anhydroglucose units. The NCC suspension was made by re-dispersing freeze-dried powder from hydrolysis of cellulose by applying ultrasonic treatment. The NCC used here has an average (sd = standard deviation) length and diameter of 210 (sd = 10) and 15 (sd = 4) nm respectively, and an average aspect ratio of 14 (range of 10-20) characterized by AFM imaging. The zeta potential of this particle is -45 mV dispersing in deionized water with no salt added. A more detailed characterization of this system is included in our previous work¹ which reports gelation of NCC suspension at elevated ionic strength and corresponding microstructure evolution due to particle aggregation and phase separation. Sodium chloride from Merck KGaA (Darmstadt Germany) was used to adjust the ionic strength. Diluted samples were produced using deionized water produced by reverse osmosis water system, which has a resistivity of 18.2 M Ω .cm (Sartorius Stedim).

Sample preparation: The suspension was prepared by diluting the 11.9 wt% NCC with deionized water to achieve the desired solid content. The ionic strength of each suspension was adjusted by adding pre-prepared 5 M NaCl solution into the NCC suspension using pipette. The volume increase necessary to achieve the highest ionic strength (0.1 M) used here was ~2%. All samples prepared were rested for 24 hours before testing. The pH value for all samples ranges from 6 to 6.2. Unless specified otherwise, materials were maintained at room temperature.

Optical observation: Cross polarized photographs are taken with the sample placed between two polarizers. A Cannon 70D camera was used. Polarizers were from Edmund Optics, and specified for light transmission across two polarizers with perpendicular axes of =0.1%. A panel LED backlight from Edmund Optics with a color temperature 6500K and <1% difference in light intensity over the panel was used. Samples were aged for 20 days before observation. Crossed polarized micrographs were prepared using an Olympus BX40 microscope equipped with polarizers above the light source and a polarized filter before the image sensor.

Rheology measurement: Rheology was measured at Anton-Paar MCR-502 compact modulus rheometer. $\text{\O}50$ mm steel parallel plate geometry was used with 1 mm gap for measurement to determine the phase diagram (Fig. S2). To prevent evaporation, silicone oil was placed on the edge of the plate during tests. Oscillatory tests were conducted for all samples for frequencies of 100 to 0.1 rad/s. The strain during testing was within the linear viscoelastic region, which was determined by performing a strain swap test. 0.5 % strain was found to be suitable for this composition range of NCC samples. Stress sweeps were conducted for stresses from 0.1 to 1000 Pa. The yield stress was determined graphically as the intercept of tangent lines of the low-shear plateau and the decline on a viscosity vs. stress plot. Cone and plate geometry ($\text{\O}50$ mm) was used to apply homogeneous shear through the sample to investigate the mechanical strength-preshear rate relation. Samples were pre-sheared at the specified shear rate until their viscosity reached equilibrium. The shear was then stopped, followed by the oscillatory test at 1 rad/s and 0.5% strain until the recorded G' and G'' reached equilibrium. The frequency sweep oscillatory test was then performed for the sample for frequencies of 100 to 0.1 rad/s. A glass base was used for samples needing cross-polarized photography.

Construction of phase diagram: The phase diagram of NCC suspension in Fig. S2 is mapped according to rheology and birefringence. The liquid-solid boundary was determined by the point at which $\tan(\delta)$ (G''/G') is independent from frequency, i.e. the gelling point due to self-similar relaxation,² which has been depicted in our previous work.³ Phase anisotropy was determined by birefringence: under cross-polarized lighting the ordered phase is bright and the isotropic phase is dark. The presence of re-entrant liquid crystal phase was confirmed with polarized micrographs (Fig. S1) following method depicted in literature.⁴

Small Angle X-ray Scattering (SAXS): NCC suspensions and hydrogels were characterised at 25 °C using small angle x-ray scattering (SAXSess mc², Anton-Paar, Austria). The x-ray ($\lambda=0.1542$ nm) was incident from a 40kV generator. The obtained 2D SAXS data was converted to 1D scattering curve using Saxesquant software by radial integration. The background scattering (for DI water with according salinities) was subtracted from SAXS data before analysis in Saxesquant software.

Supplementary Text

To the best of our knowledge, except few exceptions,^{4, 5} there are almost no studies about characteristics of re-entrant liquid crystal phase present at high ionic strength in colloidal suspensions (as shown in Fig. S1). As depicted in the main text, this behavior displays promising properties with various potential applications. However, the origin of the re-entrant liquid crystal phase before the gelation is not completely understood. From many literatures of charged colloid rods such as virus, DNA and laponite,⁶⁻⁹ the increasing ionic strength trends to destabilise chiral nematic phase by reducing double layer and screening surface charge. The thinner double layer and reduced surface potential generally results in a less twisted state, which eventually leads to an isotropic suspension. From recent theoretical work, the coexistence of two nematic phases in the phase diagram of aqueous suspension of colloidal rods is achievable with a correct combination of particle shape and surface charge.⁵ The origin of this hypothesis is based on Onsager's theory by considering the combined influence of salinity on effective volume fraction of charged colloids according to both the Debye screening effect and the twisting effect as illustrated in Fig. i. The specific requirement is that colloid has to achieve a lowered but relatively unchanged zeta potential in a range of ionic strength, which is not always a case for virus and DNA suspensions. At this condition, the addition of salt compresses the thickness of surface hydration layer of charged colloids following Debye screening effect which reduces effective volume fraction. Nevertheless, the zeta potential is less affected, so that rods will tend to minimize the 'contact' area and reduce the interparticle repulsion when approaching each other. The twisting angle between colloidal rods thus increases, as the distance between rods is reduced due to electrostatic screening, which increases the effective volume fraction. The zeta potential as a function of solution ionic strength of NCC studied in this work has been reported in our previous work,¹ which showed exactly required trend for existence of re-entrant liquid crystal phase (reproduced as red line in figure ii). We believe that this non-monotonic change in effective colloidal volume fraction leads to the presence of re-entrant liquid crystal phase at high salinity.

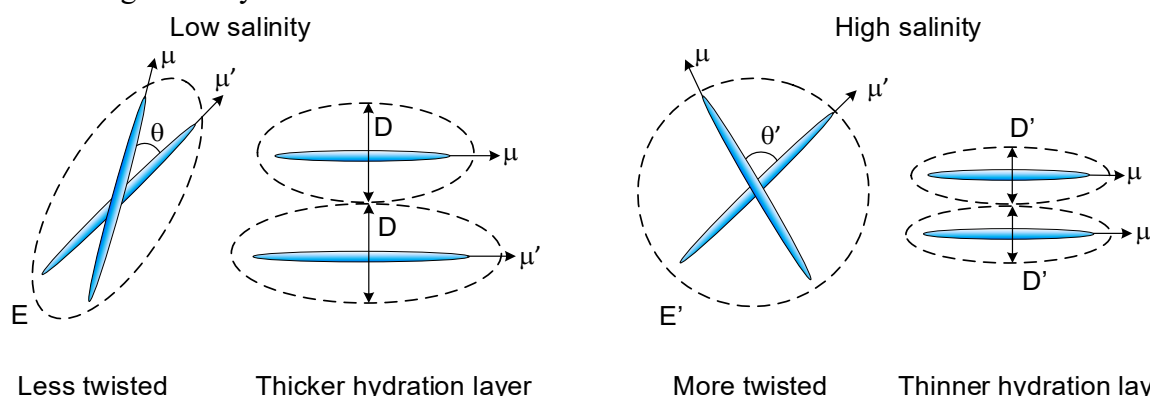


Fig. i. Schematics of influence of salinity on effective volume fraction of rod-like colloids. The concept is from reference 24 that the increased salinity causes a smaller effective diameter ($D' < D$) but a larger twisting angle ($\theta' > \theta$) between rods μ and μ' . It leads to a non-monotonic change in effective volume fraction (E) as a function of salinity.

Besides above scheme, the presence of the liquid crystal hydroglass phases is also affected by the balance between electrostatic repulsion and van der Waals forces, which controls the aggregation/ gelation of the colloidal system. Liquid crystal phase below the critical salinity for the gelation is necessary to enable phase separation occurring in an ordered phase. An example of this effect is illustrated in Fig. ii below, showing a hypothetical phase diagram of colloidal rods ($L=200\text{nm}$, $D=15\text{ nm}$) for a range of compositions comparable to our experimental conditions, determined from by approaches described in literatures.^{5, 10} The isotropic (I)-nematic (N) phase boundaries of three types of dependency of colloidal rod zeta potential on the salinity. We also roughly show liquid-solid (L/S) boundaries in the diagram calculated from jamming volume fraction (line A) and critical flocculation concentration (line B). Dependency of zeta potential on salinity (red, green blue on insert) determines the relative position of I/N boundaries and L/S boundaries. Materials marked by red and green lines can form a liquid crystal hydroglass, as the gelation line B located at nematic region. Therefore, besides a proper aspect ratio, a particular zeta potential-salinity relationship is required for a re-entrant nematic phase to coincide with the gelation, in order to fabricate a LCH. This zeta potential-salinity relationship is ultimately tunable by modification of the colloidal surface or using different type of salts.

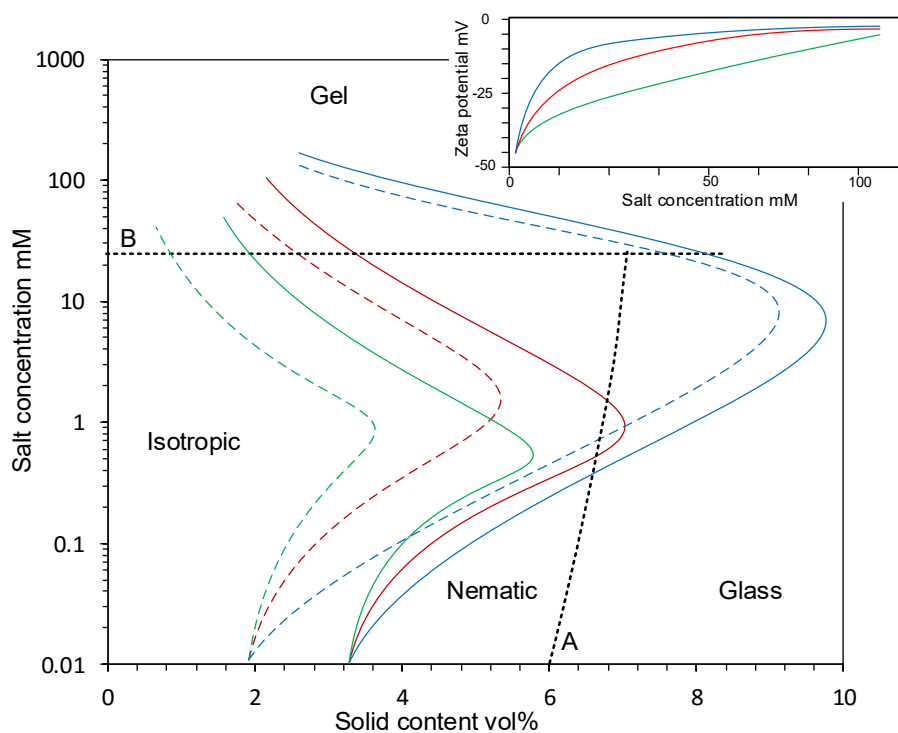
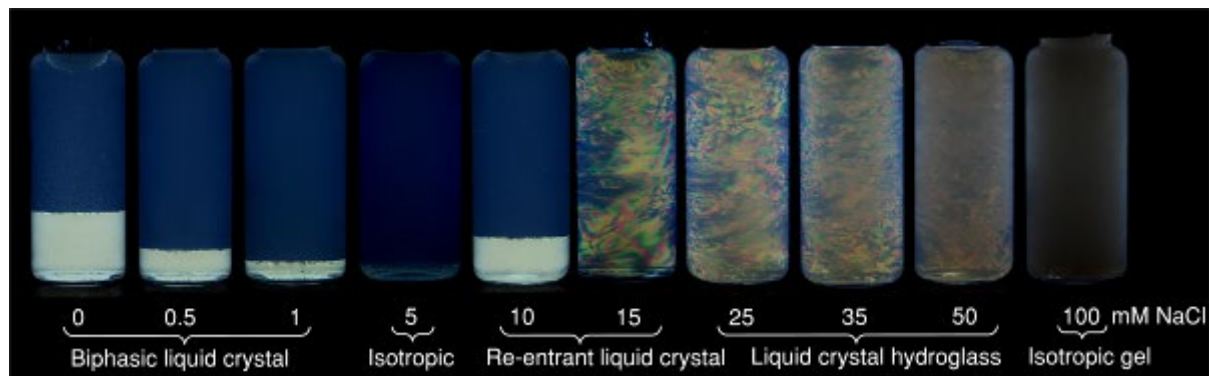


Fig. ii. Hypothetical phase diagram for colloidal rods in aqueous suspension with different salinities. It is drawn following the method in reference.^{5, 10} Solid line is the boundary of nematic phase while the dashed line is that of isotropic phase. The area between solid and dashed lines is the region where nematic and isotropic phases coexist. The colors (blue, red and green) are corresponding to the zeta potential dependency on salinity (small insert at top right). Dotted lines are hypothetical liquid-solid boundaries that line A is according to the jamming volume fraction of colloidal rods while line B is the critical flocculation concentration largely representing the gelation line. The zeta potential dependency on salinity affects the isotropic-nematic transition. Phase boundaries resulted from red and green curves show a nematic region below gelation enabling the presence of liquid crystal hydroglass. Blue curve show a I/N transition at a salinity higher than that is required for gelation, which make the phase separation occur at an isotropic state resulting in an isotropic gel.

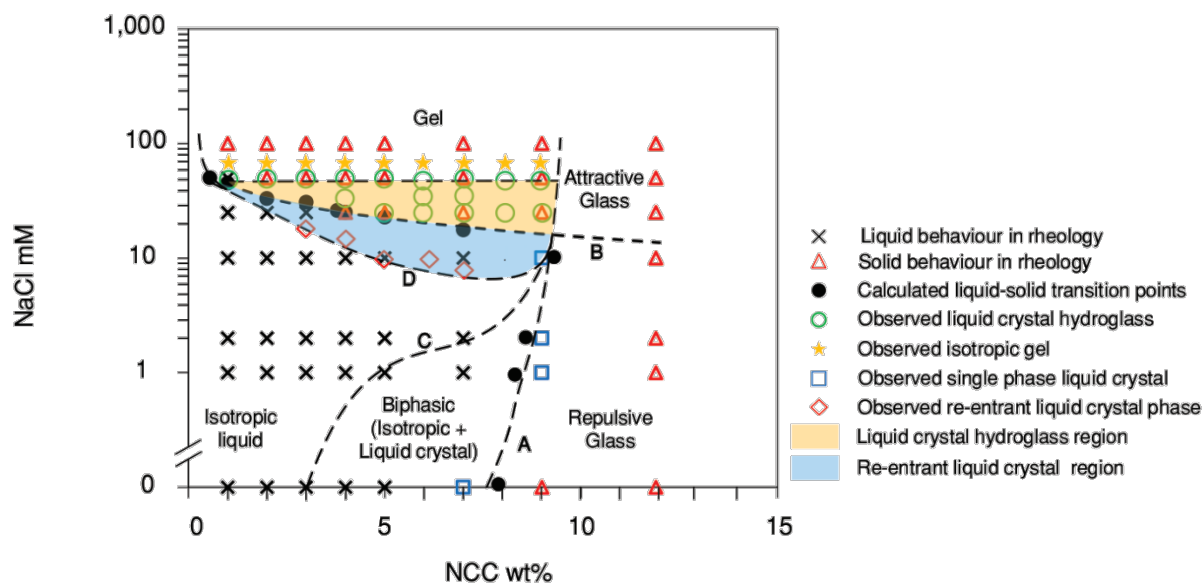
Supplementary Fig.s S1-S6

Supplementary Fig. S1- S6 as following is cited in the main text in series. A description of main features of the picture is included in the caption.

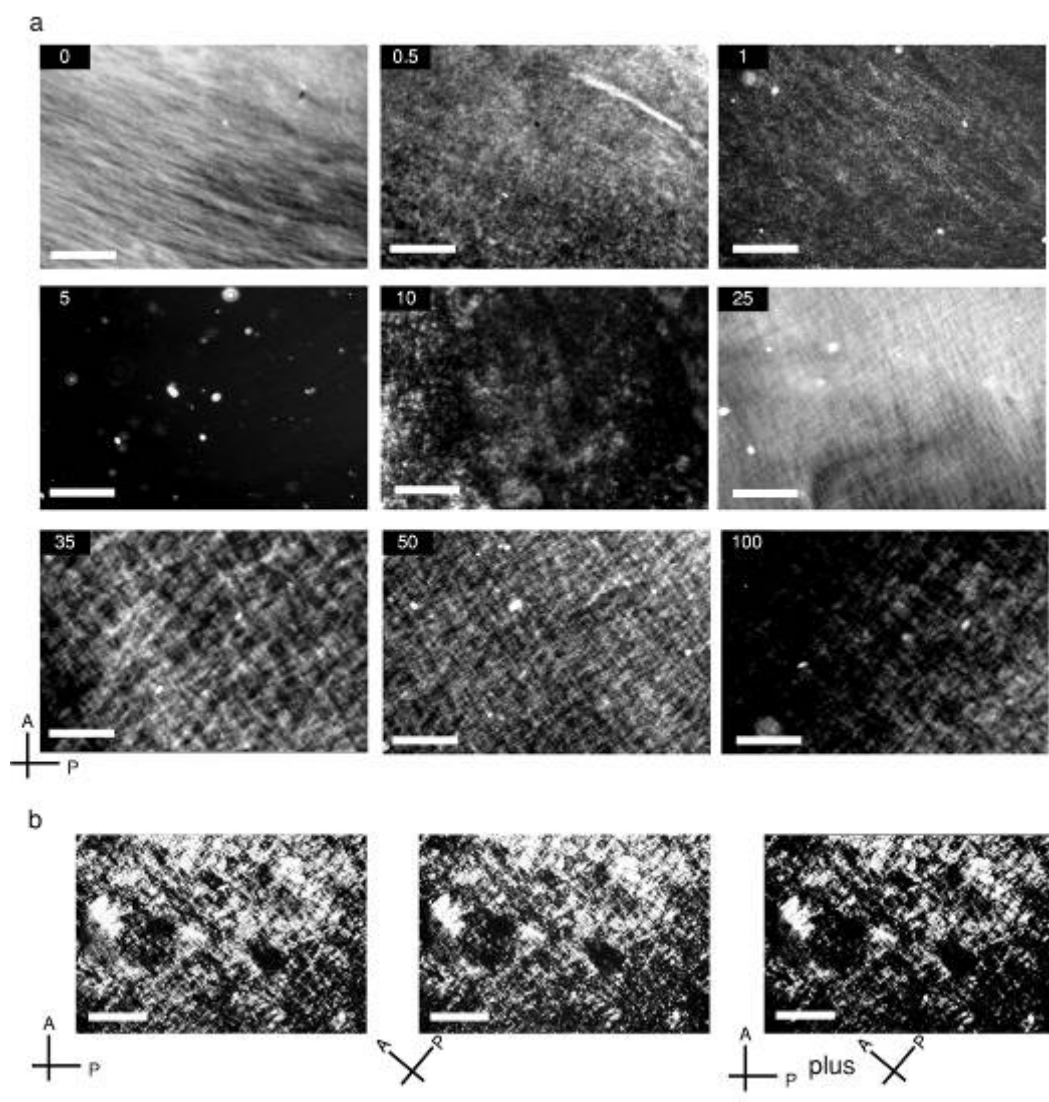


Supplementary Fig. S1. Cross-polarized Photographs of 5 wt% NCC suspensions.

Photographs of 5 wt% NCC suspension taken between crossed polarizers for varying NaCl concentration (increasing left to right, in mM). The liquid crystal phase is replaced with isotropic phase with increasing ionic strength, followed by formation of a re-entrant liquid crystal phase similar to literature reports.⁴ The birefringent liquid crystal hydroglass forms at ionic strength 25-50 mM NaCl equivalent. The isotropic gel present at 100 mM is dark due to lack of an ordered phase.

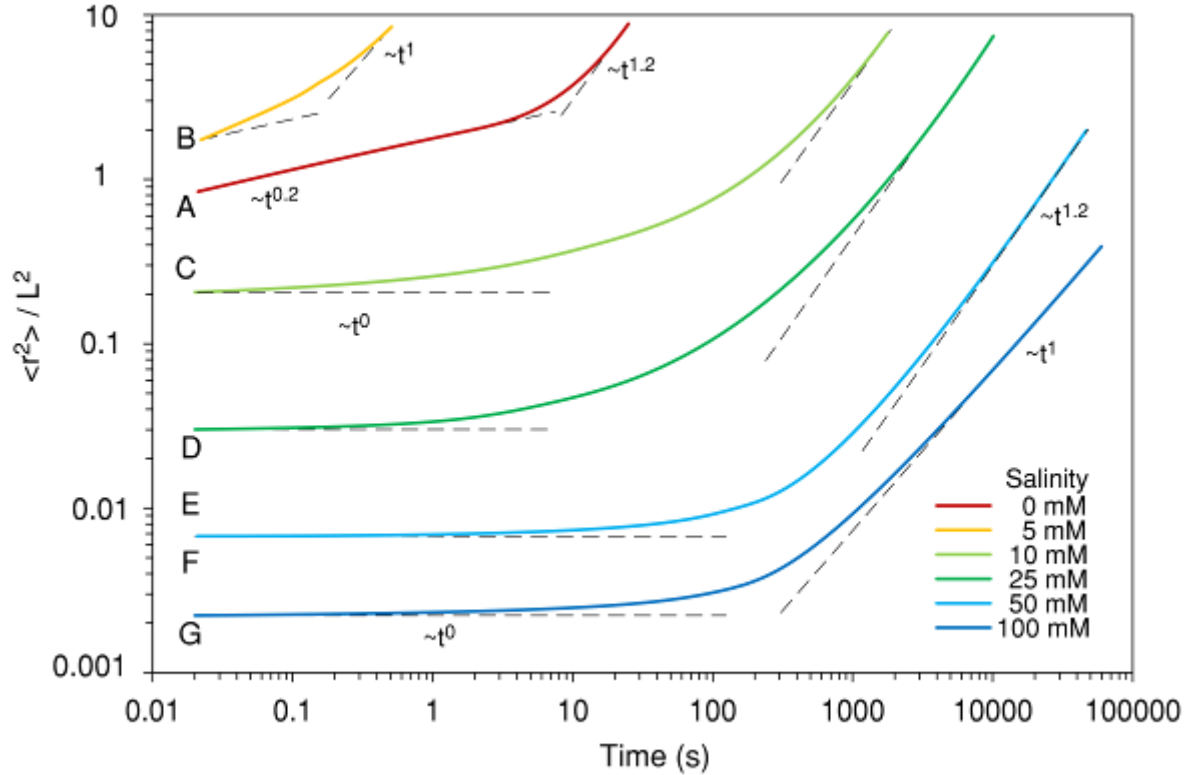


Supplementary Fig. S2. Concentration-salt phase diagram of NCC aqueous suspension. Concentration-salinity phase diagram of NCC colloidal suspension determined by rheological measurements and birefringence. Points correspond to evaluated samples, with shape indicating characteristic rheological behavior or optical signature (as per the legend). Line A and B are liquid-solid boundaries determined from rheological measurements corresponding to self-similar relaxation' (Methods). Line C and D are the boundaries between ordered and disordered region determined from birefringence. The region in yellow represents the liquid crystal hydroglass while the blue region is the re-entrant liquid crystal phase. Note that the single phase liquid crystal (marked as blue squares) is present within a very narrow range of compositions and is almost coincides with the liquid-solid transition points (black circle), and consequently is not depicted as a distinct region as it is in Fig. 1a.

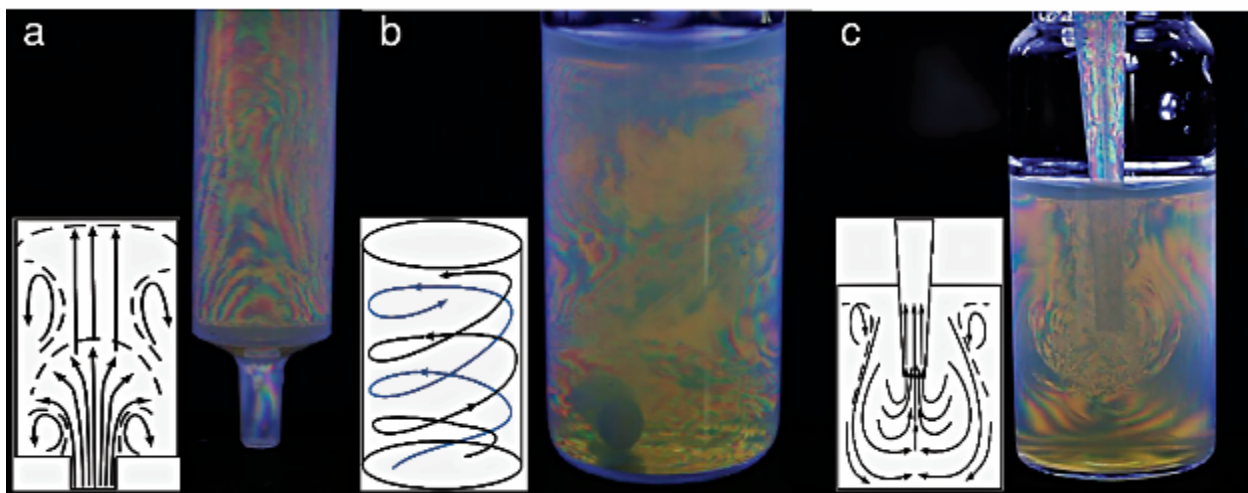


Supplementary Fig. S3. Cross-polarized micrographs of 5 wt% NCC suspension.

(a) Cross-polarized micrographs of 5 wt% NCC suspension at varying NaCl concentrations noted in values of mM for each formulation. Scale bars represent 100 μm . Bright regions correspond to ordered phase while dark correspond to isotropic. The liquid crystal hydroglass (25-50 mM) contains a dense dark phase interpreted as a structural network of isotropic attractive glass phase with a co-existing bright ordered phase. The proportion of bright region decreases with ionic strength from 25 to 100 mM indicating an evolution of mesostructure, i.e. increased relative contribution of attractive glass phase at higher salinities. (b) Cross-polarized micrographs with various angle of polarizers' axis for 5wt% NCC with 35 mM NaCl. Picture taken from conventional configuration of polarizers (left) and from polarizers rotated by 45° (middle) are multiplied in Adobe Photoshop. In the resultant picture (right), the bright region means the region that is bright in both configurations of polarizers while the dark region means that it is dark in at least one configuration of polarizers. It can be seen that bright region is still observable for a reasonable proportion after rotating polarizers' direction and multiplying pictures from two directions. It eliminates the doubt that the dark regions in polarized optical micrographs of LCHs are from rods in parallel orientation to one polarizer, and further confirms this biphasic structure consisting of an LC phase and an isotropic phase.

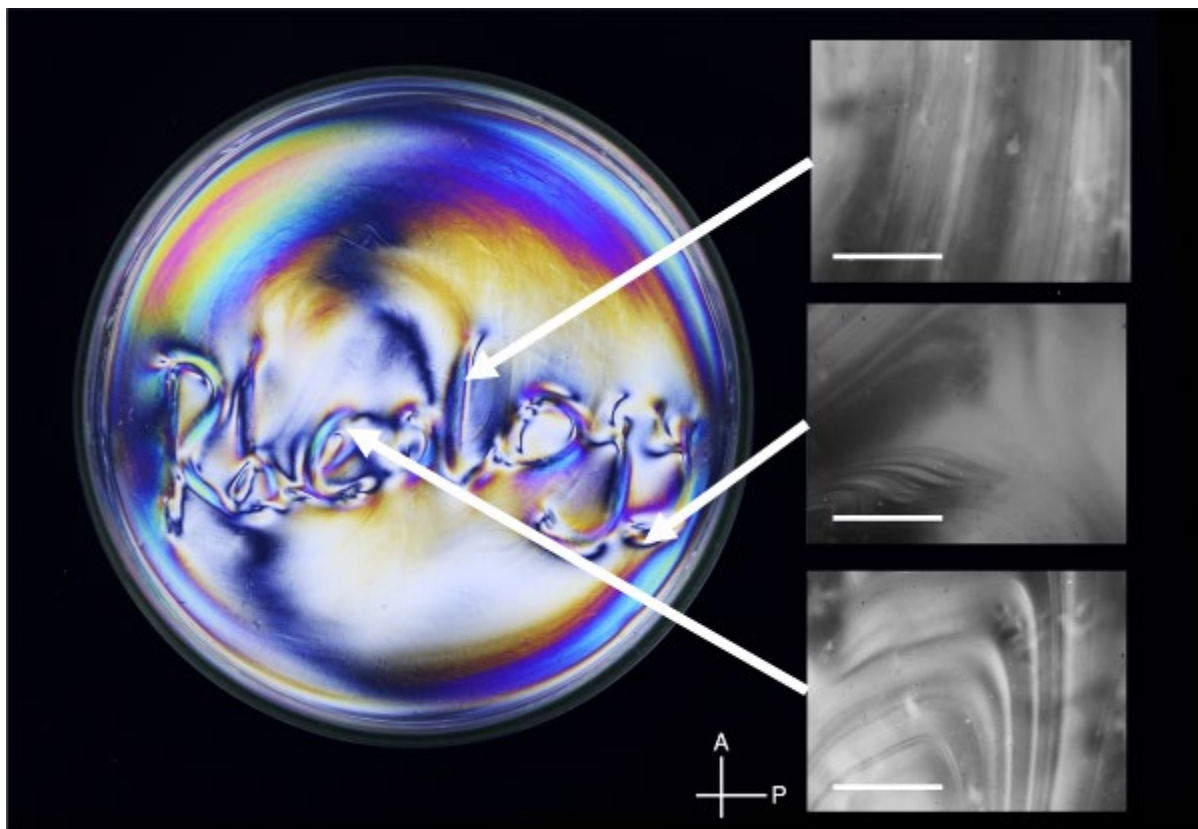


Supplementary Fig. S4. Mean squared displacement (MSD) of 5 wt% NCC suspensions. Mean squared displacement ($\langle r^2 \rangle$) of 5 wt% NCC suspension at different salinities measured via diffusive wave spectroscopy (DWS). A curve with gradient 1 indicates pure diffusional motion, and a plateau corresponds to a localization length: the characteristic distance a particle moves before it encounters an obstacle. The $\langle r^2 \rangle$ value of the plateau represents the scale of the obstacle and provides a comparative measure of the network density in gelled systems. The NCC suspension demonstrates liquid-like behavior at salinity of 1 mM. The decrease in plateau values with increasing salinity from 25 to 100 mM, representing increasing network density in agreement with observations in Fig. S3. The plateau value of an ideal attractive glass with $\langle r^2 \rangle \ll 0.01 L^2$ where L is the particle size.¹¹ The super-diffusion ($\langle r^2 \rangle \sim t^{1.2-1.5}$) is observed in liquid crystal suspensions due to the yielding nature of nematic phase.¹² This diagram indicated the biphasic structure of LCHs in terms of their slow dynamics.



Supplementary Fig. S5. Complex structural alignments introduced by flow fields.

Complex structural alignments introduced by (a) expansion flow (loading sample into a syringe), (b) helical flow (stirring with a magnetic stirrer), and (c) suction flow (using a pipette). Photographs were taken between crossed polarizers 2 hours subsequent to imposing the flow field. The flow-induced structure visible with polarized light is maintained by the characteristic ‘cells and frame’ structure of the LCH. Inserts are the schematics of respective flow patterns.



Supplementary Fig. S6. Spatially heterogeneous structural anisotropy induced by heterogeneous flow.

An example of a spatially heterogeneous pattern induced by heterogeneous flow. A word “Rheology” is drawn on the LCH and the cross-polarizer photograph and micrographs are 2 hours later. Micrographs correspond to positions indicated by white arrows (edge of letters). As in Fig. 2, the surface of the gel relaxes, with relevant internal structures only visible under polarised light. Scale bars are 100 μm . The structural ordering of this material is programmable by the flow field in an almost arbitrary way, enabling simple introduction of spatial heterogeneity.

1. Y. Xu, A. D. Atrens and J. R. Stokes, *Journal of colloid and interface science*, 2017, **496**, 130-140.
2. H. H. Winter and M. Mours, in *Neutron Spin Echo Spectroscopy Viscoelasticity Rheology* Springer Berlin Heidelberg, Berlin, 1997, vol. 134, pp. 165-234.
3. Y. Xu, A. D. Atrens and J. R. Stokes, *Soft matter*, 2018, **14**, 1953-1963.
4. A. Hirai, O. Inui, F. Horii and M. Tsuji, *Langmuir*, 2009, **25**, 497-502.
5. T. Drwenski, S. Dussi, M. Hermes, M. Dijkstra and R. van Roij, *J Chem Phys*, 2016, **144**, 094901.
6. X. M. Dong, T. Kimura, J.-F. Revol and D. G. Gray, *Langmuir*, 1996, **12**, 2076-2082.
7. Z. Dogic and S. Fraden, *Langmuir*, 2000, **16**, 7820-7824.
8. K. Kang, A. Wilk, A. Patkowski and J. K. Dhont, *J Chem Phys*, 2007, **126**, 214501.
9. N. K. Reddy, Z. K. Zhang, M. P. Lettinga, J. K. G. Dhont and J. Vermant, *Journal of Rheology*, 2012, **56**, 1153-1174.
10. R. v. Roij, *European Journal of Physics*, 2005, **26**, S57-S67.
11. E. Zaccarelli, S. V. Buldyrev, E. La Nave, A. J. Moreno, I. Saika-Voivod, F. Sciortino and P. Tartaglia, *Physical review letters*, 2005, **94**, 218301.
12. M. M. Alam and R. Mezzenga, *Langmuir*, 2011, **27**, 6171-6178.